العدد 16 شباط 2025
المجلة العراقية للبحوث الإنسانية والإجتماعية والعلمية
Iraqi Journal of Humanitarian, Social and Scientific Research
No.16 Feb 2025
Print ISSN 2710-0952 Electronic ISSN 2790-1254

Mechanical Stability, Electronic and Optical Properties of HfX2 (X=S, Se, Te): A DFT Study

Hussein Ghmaies Ied

Abstract

Based on the density functional theory, mechanical, electronic and optical stability characteristics of HfS2, HfSSe, and HfSTe compounds have been investigated. The mechanical results show that all three cases have ground state point and equilibrium volume. The derivative of bulk modulus these compounds indicates the presence of strong covalent bonds in them. The phonon dispersion of these compounds shows that all of them have dynamic stability. All three 2D HfS2, HfSSe, and HfSTe compounds are semiconductors with indirect band gaps of 1 and 1.3, and 1.1 eV, respectively. Their dielectric functions show that all three compounds have the highest response to visible light in the visible region.

Keywords: DFT, 2D HfX2 (X=S, Se, Te), Electronic properties, Optical properties.

الاستقرار الميكانيكي والخواص الإلكترونية والبصرية لمركبات HfS2 (X=S, Se, Te): دراسةDFT

الباحث: حسين غميس عيد

الملخص

استنادًا إلى نظرية الكثافة الوظيفية، تم التحقيق في خصائص الاستقرار الميكانيكي والإلكتروني والبصري لمركبات HfS2 و HfSSeو .HfSTeتظهر النتائج الميكانيكية أن جميع الحالات الثلاث لها نقطة حالة أرضية وحجم توازن. يشير مشتق معامل الكتلة لهذه المركبات إلى وجود روابط تساهمية قوية فيها. يُظهر تشتت الفونون لهذه المركبات أن جميعها تتمتع باستقرار ديناميكي. جميع المركبات الثنائية الأبعاد HfS2 و HfSSeو HfSTeالثلاثة هي أشباه موصلات ذات فجوات نطاق غير مباشرة تبلغ 1 و1.3 و1.1 إلكترون فولت على التوالي. تُظهر وظائفها العازلة أن جميع المركبات الثلاثة لديها أعلى استجابة للضوء المرئي في المنطقة المرئية.

الكلمات المفتاحية: DFT، 2D HfX2 (X=S, Se, Te)، الخواص الإلكترونية، الخواص البصرية.

1. Introduction

Due to the unique electronic and optical behaviors, in recent years, much attention has been paid to two-dimensional structures (2D) [1-3]. After the discovery of graphene, the search for graphene-like 2D structures intensified and these compounds quickly attracted the attention of researchers and industries [4]. The zero band gap of graphene has been bottleneck for its electronic applications [5–9], which led to the discovery of other 2D materials having non-zero band gap [10–

16]. Among 2D materials, the latest research is being focused on non-zero band gap layered Transition Metal Dichalcogenides (TMDCs) of formula MX2 (M = Transition Metal, X = Chalcogen), e.g., MoS2 monolayer, a Group VI TMDC have a direct band gap of 1.8 eV [12]. Several MXene structures have been fabricated nowadays and these materials have been explored theoretically. A recent review about the 2D MXenes structures and their properties can be found in Ref. [11] where their potential applications, such as in the fields of energy storage, sewage disposal, electromagnetic interference shielding, nuclide adsorption, catalysts, sensors, composite materials, and electronics have been discussed. Moreover, the various biomedical applications of two dimensional Mxenes were pointed out in [11]; see also [12-15] and references therein. TMDCs compounds are expected to be widely used for FETs, hydrogen storage, Li-ion batteries and biosensors [17–26] applications. Group IV TMDC (HfX2, ZrX2) compounds are a suitable alternative to other reported TMDCs so far due to their high current density and good mobility [27-30]. One of the 2D cases for the photodetectors and solar cell applications is ZrS2 with 1.1eV band gap [31,32]. The existence of crystal defects in the arrangement of ions is one of the problems of TMDCs compounds in contrast to their unique characteristics. Crystalline defects are generally formed in the layered material during their synthesis [33,34], and their nature and its effect depend upon the synthesis process, for example, MoS2 grown by CVD process has much lower mobility than that of mechanically exfoliated ones [35]. Recently, HfSe2 monolayers have been successfully synthesized and used in transistors. However, there is still no study on the effect of vacancy on the physical properties of HfSe2, which motivated us to investigate the effect of the defects on its electronic and magnetic properties. We also investigated systematic substitutional defect studies on the electronic and magnetic properties of monolayer HfSe2 by 4d and 5d TM using first-principles calculations.

2. Computational Methods

The structural, electronic and optical properties of HfS2, HfSSe, and HfSTe mono-layers have been calculated based on density functional theory (DFT) and first principle computations where the problem of many interactions between electrons and nuclei is reduced to a single electron equation. We have employed the Wien2K [36], Quantum Espresso [37] codes. Solving the Kohn-Sham equations is done using the full-potential linearized augmented-plane wave (FP-LAPW) method, which is used in the Wien2K package.

The exchange-correlation potential of the Kohn-Sham equation has been approximated by the generalized gradient approximation (GGA) [38-40]. In order to perform the structural and electronic computations, the KPoint, RKmax and

Gmax optimized parameters have been selected as $16 \times 16 \times 1$, 8.5, and 13.5, respectively in the Wien2K software. The atomic forces have been optimized up to 10^{-6} (dyn/a.u.) accuracy. In order to calculate the phonon dispersion of our structure the Quantum Espresso software has been employed and the optimized *k*-point and *q*-point meshes for phonon computations have been selected as $10 \times 10 \times 2$ and $5 \times 5 \times 1$ respectively.

3. Results

3.1. Structural Properties

In Figure (1), the schematic diagram of the crystal structure of two-dimensional HfX2 compounds is shown, where the position of X atom can be replaced by S, Se, or Te atoms. In this research, we compared the structural and electronic characteristics of HfS2, HfSSe, and HfSTe compounds by substituting the Se, and Te atoms to the S atom. The three mentioned atoms are all in the sixth column of the periodic table and have similar electronic characteristics, so their orbital structures are S, [Ne] $3s^2$ $3p^4$, Se, [Ar] $4s^2$ $3d^{10}$ $4p^4$ and Te, [Kr] $5s^2$ respectively. $4d^{10}$ $5p^4$, As can be seen, their valence layer has a full s orbital with two atoms and a half-filled p orbital with 4 electrons. But the Se and Te also have full d orbitals in this layer. On the other hand, the atomic weight and the number of electrons in the core layer and close to the nucleus in Te are smaller than the other two, and Se is larger than S. Therefore, due to the closeness of the electronic behavior of these atoms, it is predicted that their replacement will be possible and there will be no problem in the stability of these nanostructures, which will be discussed in the following. As can be seen from figure (1), their unit cell is hexagonal and its edges are zigzag. The Hf atom is also one of transition metal atoms with orbital structure [Xe] $6s^2$ $4f^{14}$ $5d^2$, which has a half-filled d orbital, which is why it is considered an active metal and can create strong bonds in connection with the half-filled p orbitals of S, Se, and Te atoms. In figure (2), the electron density of this atom is shown and it can be seen that the electron density around it has a large electron gradient and has given it the possibility of strong activity.

To prove the stability of any structure, first its mechanical stability must be checked from a static and dynamic point of view. In Figure (3), we have drawn the energy diagrams of the unit cell in terms of volume for the three named compounds. The graphs show that there is a minimum point in all three structures, which indicates the existence of an equilibrium volume. In these three graphs, we can see the steep slope of the graphs, which is representative of the large bulk modulus for them, and on the other hand, these curves are relative to the minimum point of symmetry. The results of these three graphs in table (1) show their crystal hardness. Also, the values obtained for the bulk modulus derivative show that they

have covalent bonds, although the bond strength between atoms in HfSSe is higher than other compounds. Also, the specifications of the unit cell of these compounds are listed in Table (1).

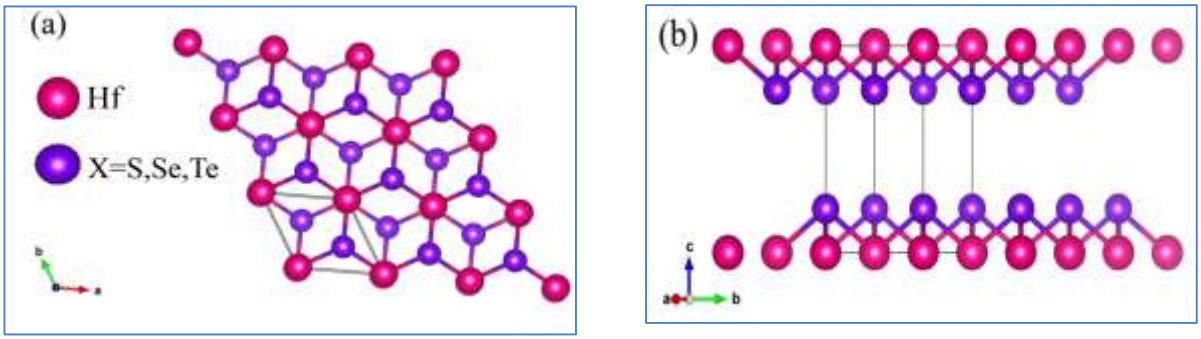

Figure (1): The crystal structure schematic of HfX2

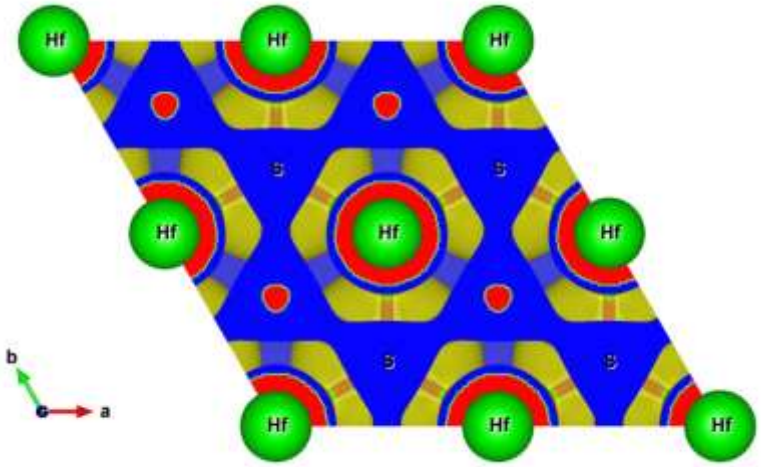

Figure (2): The electron density on the HfX2

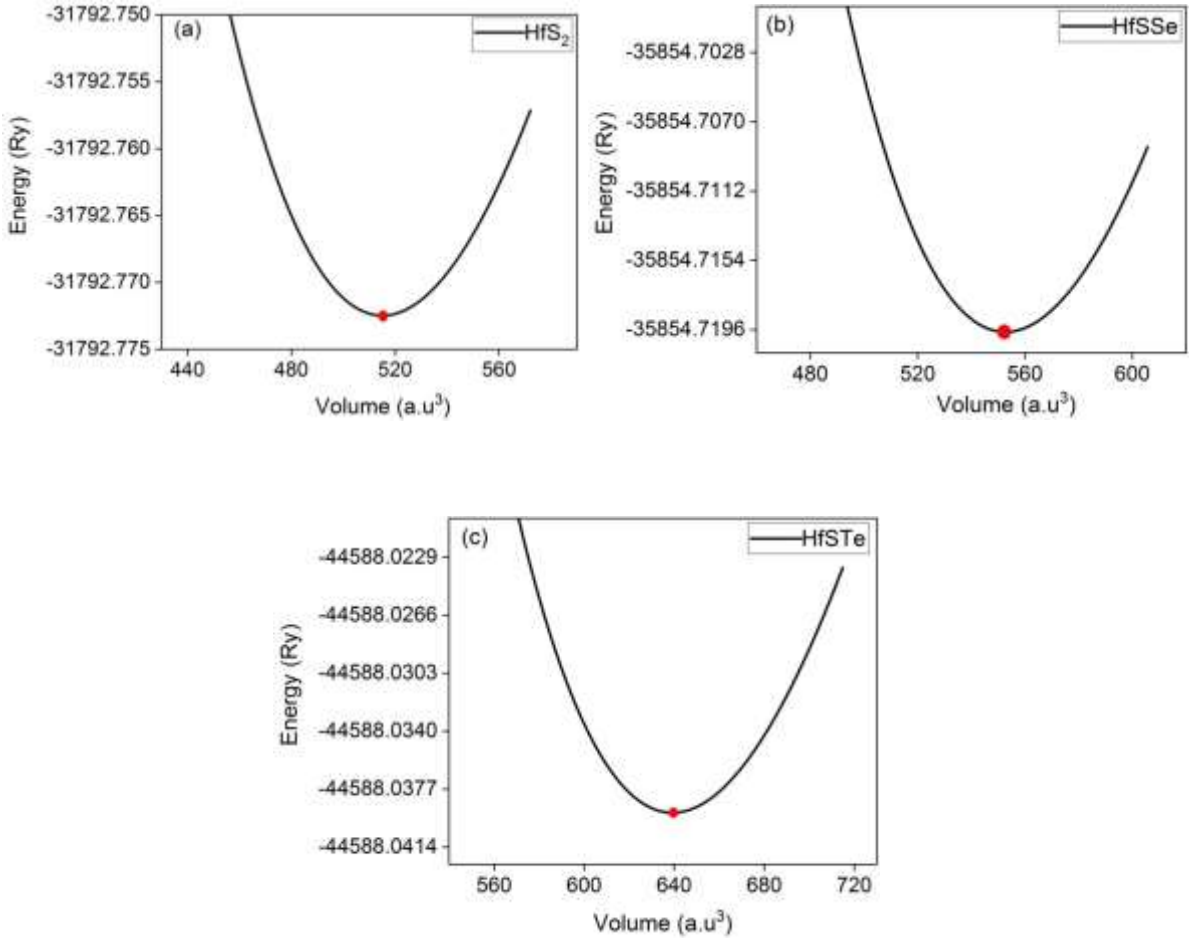

Figure (3): The energy-volume diagrams of HfS2, HfSSe, and HfSTe 2D.

Table (1): The optimized lattice constants a, c (bohr), equilibrium volume B(GPa), Bulk modulus, the derivative of bulk modulus B', total energy (Ry), and energy gap (eV) of HfS2, HfSSe, and HfSTe 2D.

structure	a (bohr)	c (bohr)	Volume ($a.u^3$)	B(Gpa)	B'	Energy (Ry)	E_{gap}(eV)
HfS2	6.8849	12.4428	515.0811	83.1949	3.3297	-31792.7724	1
HfSSe	7.068	12.7733	552.6215	75.9741	4.3669	-35854.7197	1.3
HfSTe	7.4195	13.40	639.2552	62.4154	4.1468	-44588.0392	1.1

In the following, we investigated the dynamic stability of HfS2, HfSSe and HfSTe compounds. For this purpose, their phonon dispersion has been calculated in the first region along the symmetry line Γ-M-K-Γ, and the phonon band structure is drawn in Figure (4). It is noteworthy that in all three diagrams phonon levels are positive at all symmetry points, which indicates the dynamic stability of these compounds. Due to the difference in the mass of Hf and S in panel (a), we see a large frequency gap between the acoustic and optical branches from 150 cm^{-1} to 190 cm^{-1}. The gradient of the levels in the acoustic region is greater than the optical one, which indicates the ability to transmit heat in this combination, although in the optical region, it is also capable of transmitting electromagnetic waves in the infrared region. In panel (b), with the addition of a Se atom instead of one of the S atoms, we see that the frequency gap shifts to higher energies in the range of 200 cm^{-1} to 230 cm^{-1}. But energy transfer in all branches has been transferred to lower frequencies. In panel (c), by adding Te instead of Se, we see a large frequency gap from 170 cm^{-1} to 230 cm^{-1} due to its large atomic mass difference with the S atom. Therefore, these three two-dimensional structures, along with dynamic stability, are good options for heat and light transmission in the infrared range.

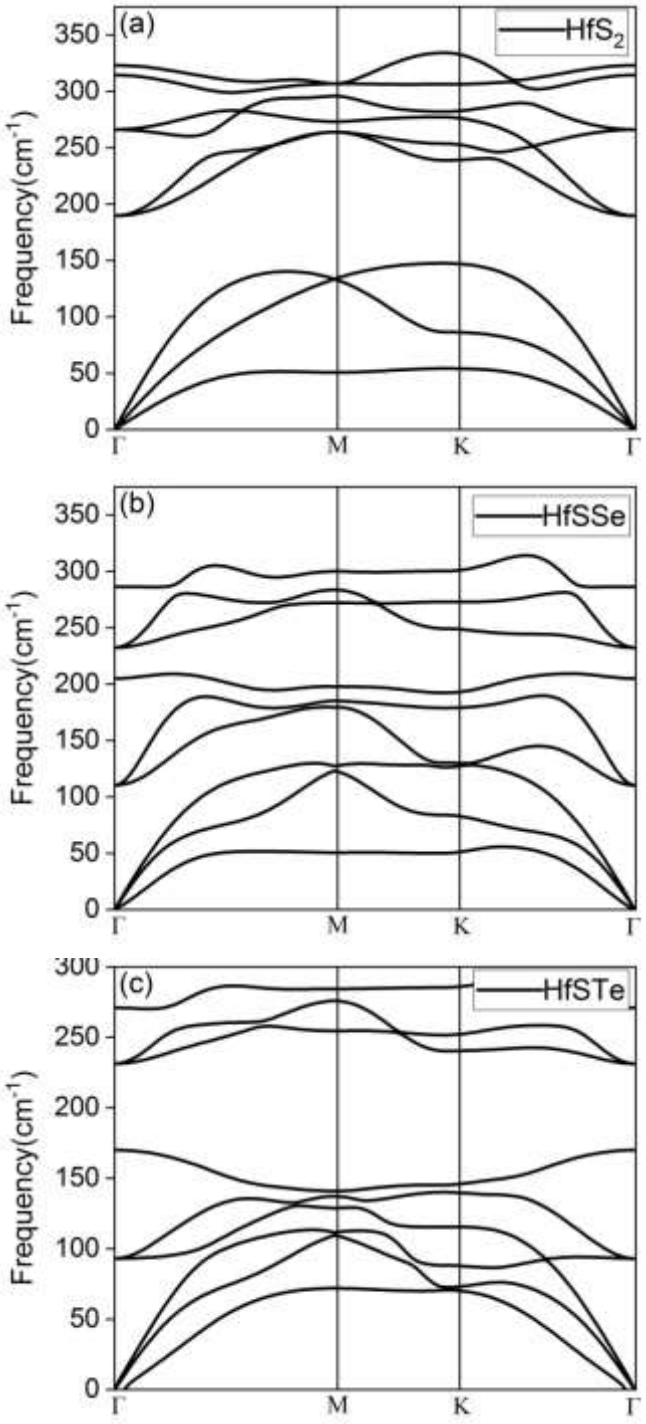

Figure (3): The phonon dispersion of the HfS2, HfSSe, and HfSTe along the Γ-M-K-Γ

3.2. The Electronic Properties

In this section, we have investigated the electronic behavior of the 2D HfS2, HfSe2 and HfSTe by depicted two diagrams of the band structure and the density of electronic states (DOS). Many physical properties of materials are due to their electronic behavior. In Figure (5-a), it is observed that the compound HfS2 is a semiconductor with an indirect band gap of about 1 eV. The electron levels in the valence region have a large slope, which indicates the high mobility of the holes when the electrons are excited. These levels, as shown by the electron state density curve, belong to S-p and Hf-d orbitals, although the contribution of p orbitals is greater. In contrast, conduction band alignments mostly belong to Hf-d orbitals. The gradient of the levels in the conduction region also indicates the high mobility of electrons. In this combination, we also see a forbidden gap for energy in the conduction area. In panel (b), we have drawn the band structure and DOS of the HfSSe compound. Here we also see an indirect bandgap of 1.3eV, and in the valence region, electron levels are mostly contributed by S-p and Se-p, and conduction levels mostly belong to Hf-d. The presence of Se atoms increases the electronic states compared to S, and as a result, the conductivity of excited electrons and holes has increased. In panel (c), it is observed that the alignments of the conduction region are closer to the Fermi level and there is an indirect energy gap of 1.1eV, but in the conduction region the gap of the previous shapes is enlarged.

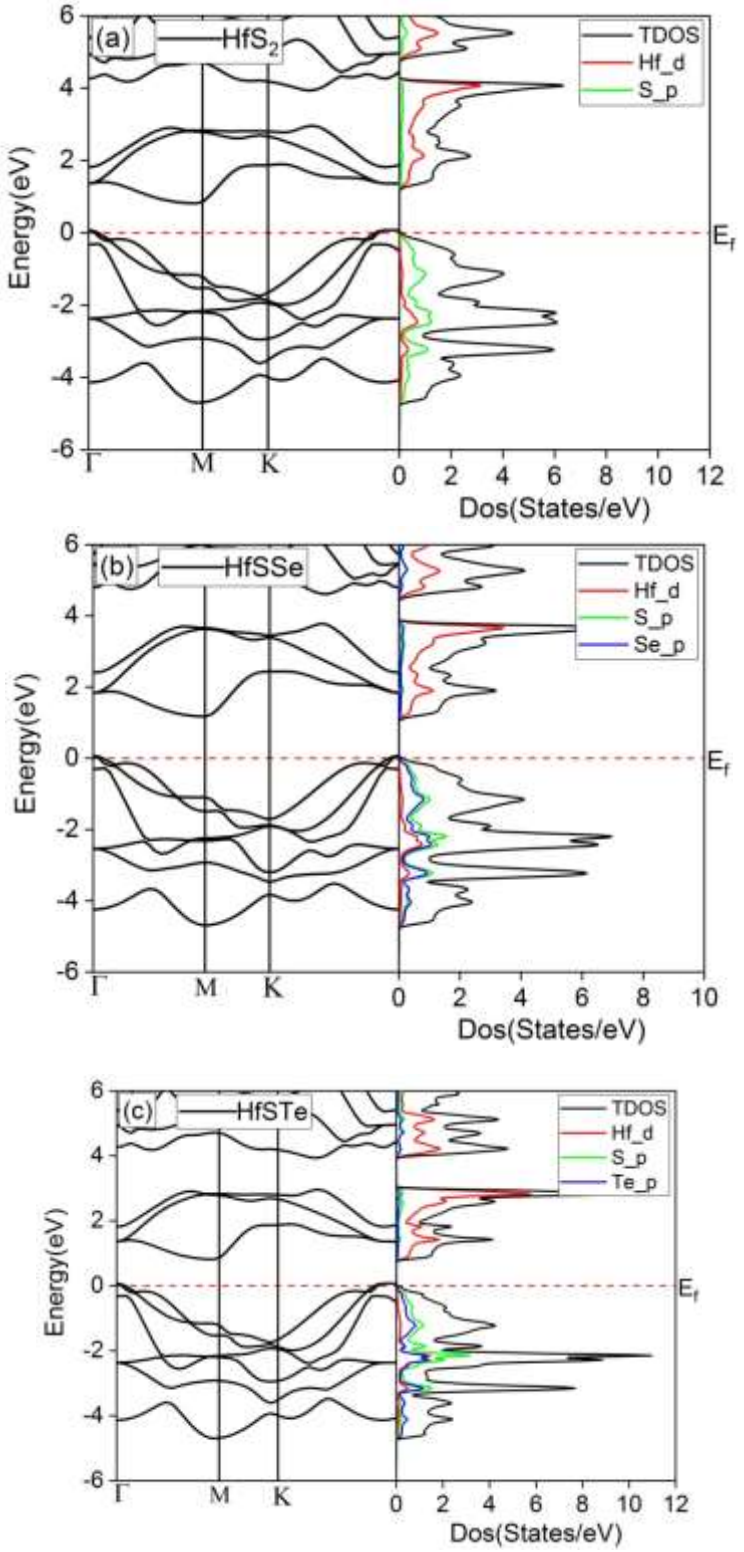

Figure (5): The bandstructure and total and partial DOS of the 2D HfS2, HfSSe, and HfSTe.

3.3. The Optical Properties

In Figure (6), the real part of the dielectric function for three compounds HfS2, HfSSe and HfSTe are drawn in two directions in the plane (x) and perpendicular to the plane (z) in terms of the irradiated photons. It has been observed in panel (a) that with the increase in the energy of the irradiated photon, the static value of the real part of the dielectric function is 6 in the z direction and 8 in the x direction, which represents semiconducting behavior in both directions. With the increase of irradiated photon, both functions have sharp peaks in the visible edge. In the x direction, this peak has fallen to a very steep slope, which is indicative of optical instability in this region. It has even become negative in the ultraviolet edge, but in the z direction, this curve has two peaks at 5eV and 7eV after one peak at the visible edge. In the x direction, it has become negative from 6.5eV onwards, and in the z direction, it has become negative from 8.5eV onwards, which indicates the appearance of plasmonic aggregations and optically unstable behavior. In panel (b), we see the same behavior for HfSSe, with the difference that the static value has increased in the x direction, which indicates the reduction of its band gap. In the same way, the behavior of HfSTe is repeated in panel (c), with the difference that the static value is still lower, which indicates the agility of electrons during excitation, and at each energy, the magnitude of this function is larger than the other two compounds.

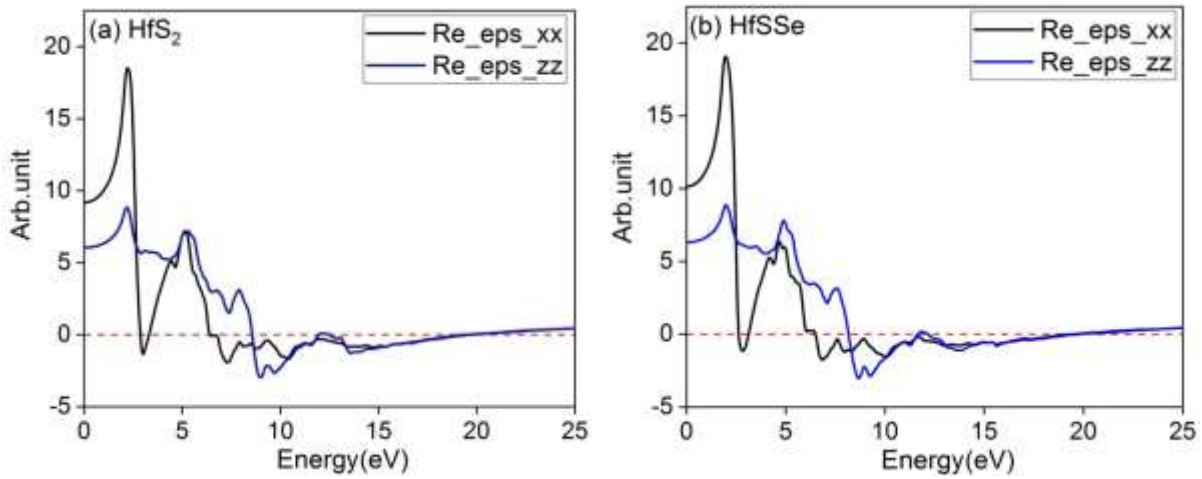

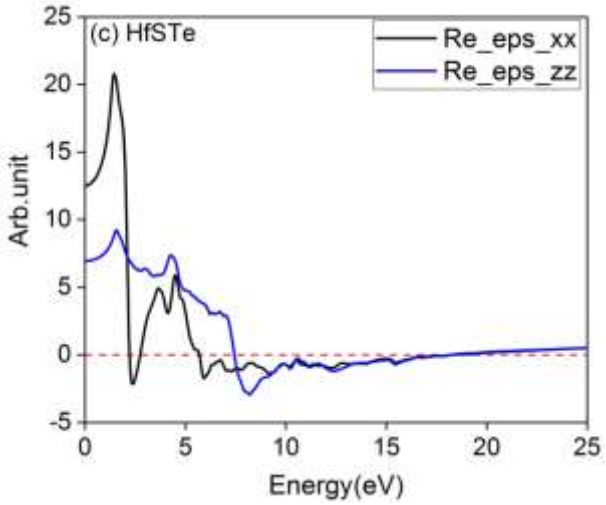

Figure (6): The Real part of dielectric function of 2D HfS2, HfSSe, and HfSTe.

In figure (7), the imaginary part of the dielectric function is displayed. This curve is directly related to the electronic structure of the substance. In all three diagrams and in both directions, we see an optical gap for these three compounds, which is in full agreement with the diagrams of band structure and density of electronic states. In panel (a), the HS2 compound in the x direction at the visible edge has a very sharp and long peak, which represents the electronic interband, and we see another peak at 6eV. But the magnitude of the peaks in the z direction has been reversed, and with the increase in the energy of the radiated photon, the magnitude of the peaks has increased. With the increase in the atomic number of the substituted atoms in panels (b) and (c), we see the magnitude of the peaks, because more energy is needed to transfer electrons from filled to empty levels. In all three cases, we see a blue shift in the peaks in the z direction.

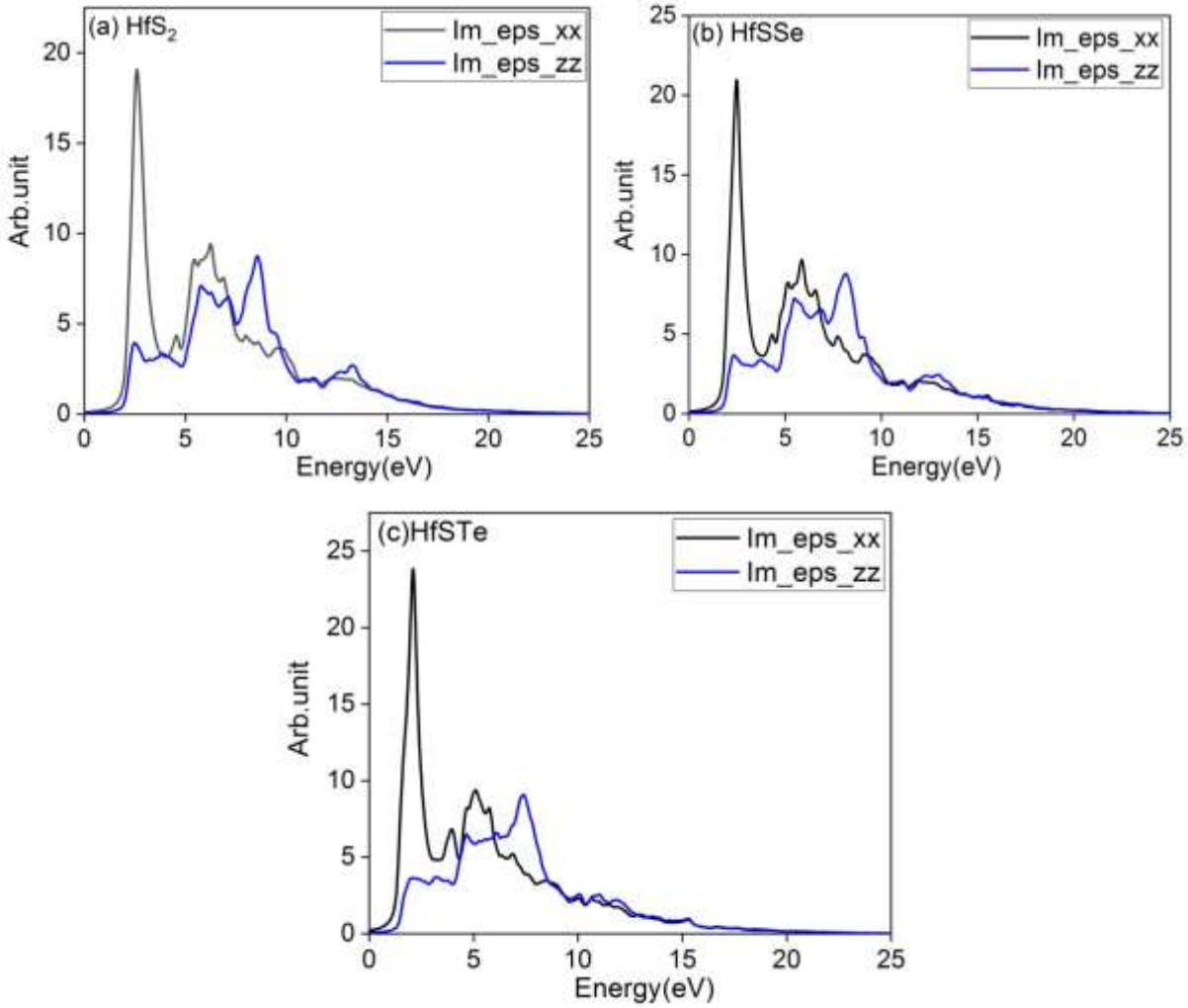

Figure (7): The Imaginary part of dielectric function of 2D HfS2, HfSSe, and HfSTe.

In figure (8), the diagram of the loss function spectrum for three compounds HfS2, HfSSe and HSTe are drawn in two directions x and z. A very important point in these three panels is that light loss occurred in all three compositions at high energies and in the range of 20eV. Therefore, according to the behavior of this compound in figures 7 and 6, we can hope that they are suitable options for use in the infrared, visible and ultraviolet edge.

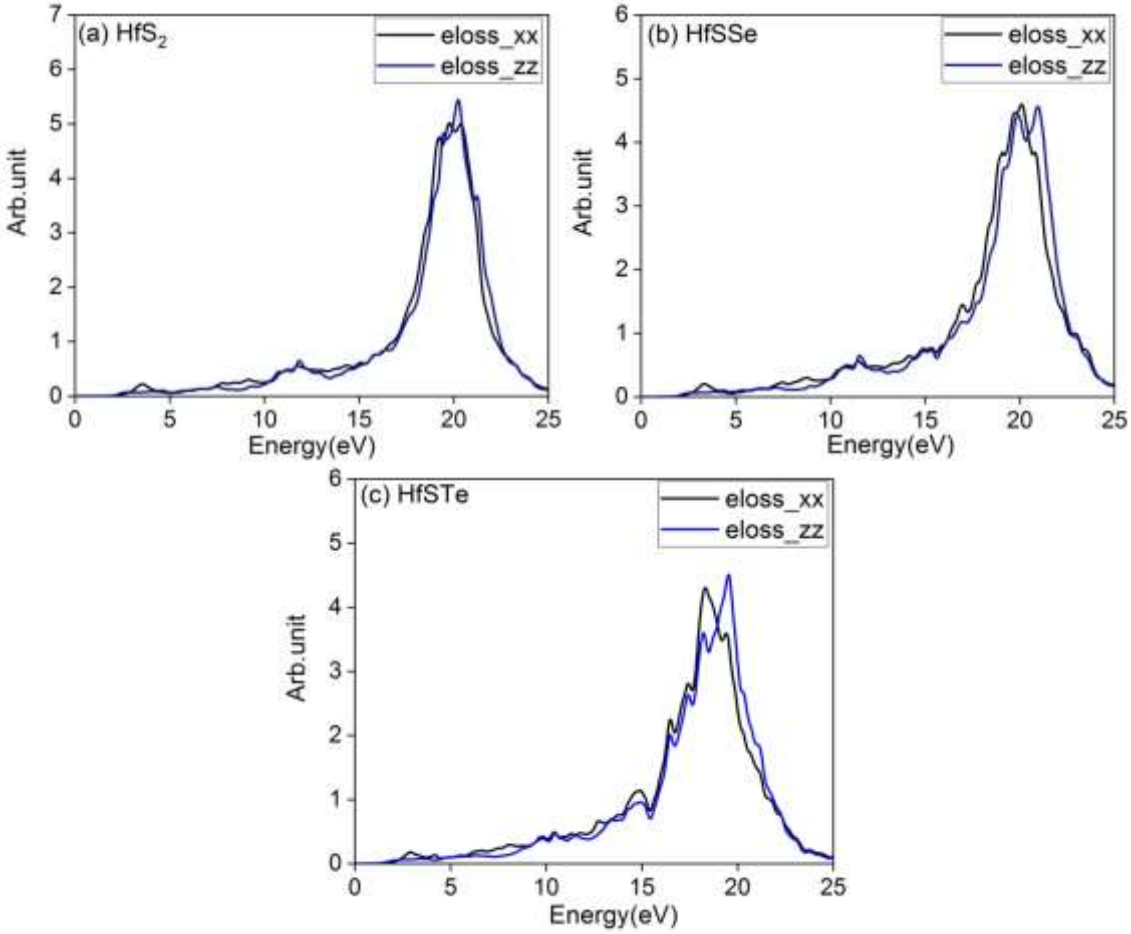

Figure (8): The energy loss function of 2D HfS2, HfSSe, and HfSTe.

4. Conclusion

Based on density functional theory calculations, mechanical stability, electronic and optical properties of 2D HfS2, HfSSe, and HfSTe compounds were investigated. The bulk modulus of these compounds represents the hardness of these crystals, and the derivative of the bulk modulus also showed that the bond between atoms is covalent, which is another indication of the stability of these crystals. The phonon band structure also indicates their dynamic stability and the mass difference between the atoms has caused a frequency gap, which of course is reduced in the alpha composition, which indicates a better heat transfer in this structure.

The 2D HfS2 Compound is a semiconductor or indirect bandgap of 1eV, which has been increased to 1.3eV by substituting the Se atom in HfSSe case. The high electron density in the range of the Fermi level shows that these compounds are very suitable for optical and electron transition applications. The static estimation of the real part of the dielectric constant confirmed the semiconducting behavior of

these compounds and their response to the light emitted was at the visible edge. At energies higher than 6 eV, their value has become negative, which indicates metallic behavior and plasmonic accumulation. The main peaks of the imaginary part of the dielectric function occurred at the visible edge, which represents the interband transfer of electrons. The loss function diagrams showed that the least loss of optical energy occurred in the visible region, which made them suitable options for optical applications in the visible and infrared ranges.

References

[1] K.S. Novoselov, A.K. Geim, S.V. Morozov, D. Jiang, Y. Zhang, S.V. Dubonos, I.V. Grigorieva, A.A. Firsov, Electric field effect in atomically thin carbon films, Science 306 (2004) 666–669.

[2] M.-H. Lee, Y. Cho, K.-E. Byun, K.W. Shin, S.-G. Nam, C. Kim, H. Kim, S.-A. Han, S.- W. Kim, H.-J. Shin, S. Park, Two-dimensional materials inserted at the metal/ semiconductor interface: attractive candidates for semiconductor device contacts, Nano Lett. 18 (2018) 4878–4884.

[3] M. Chhowalla, D. Jena, H. Zhang, Two-dimensional semiconductors for transistors, Nat. Rev. Mater. 1 (2016) 16052.

[4] A.K. Geim, K.S. Novoselov, The rise of graphene, Nat. Mater. 6 (2007) 183–191.

[5] R.R. Nair, P. Blake, A.N. Grigorenko, K.S. Novoselov, T.J. Booth, T. Stauber, N.M.R. Peres, A.K. Geim, Fine structure constant defines visual transparency of graphene, Science 320 (2008) 1308.

[6] C. Lee, X. Wei, J.W. Kysar, J. Hone, Measurement of the elastic properties and intrinsic strength of monolayer graphene, Science 321 (2008) 385–388.

[7] S.V. Morozov, K.S. Novoselov, M.I. Katsnelson, F. Schedin, D.C. Elias, J.A. Jaszczak, A.K. Geim, Giant intrinsic carrier mobilities in graphene and its bilayer, Phys. Rev. Lett. 100 (2008) 016602.

[8] K.S. Novoselov, A.K. Geim, S.V. Morozov, D. Jiang, M.I. Katsnelson, I.V. Grigorieva, S.V. Dubonos, A.A. Firsov, Two-dimensional gas of massless Dirac fermions in graphene, Nature 438 (2005) 197–200.

[9] S. Das Sarma, S. Adam, E.H. Hwang, E. Rossi, Electronic transport in two-dimensional graphene, Rev. Mod. Phys. 83 (2011) 407–470.

[10] F. Schwierz, J. Pezoldt, R. Granzner, Two-dimensional materials and their prospects in transistor electronics, Nanoscale 7 (2015) 8261–8283.

[11] M. Xu, T. Liang, M. Shi, H. Chen, Graphene-like two-dimensional materials, Chem. Rev. 113 (2013) 3766–3798.

[12] K.F. Mak, C. Lee, J. Hone, J. Shan, T.F. Heinz, Atomically thin mos2: a new directgap semiconductor, Phys. Rev. Lett. 105 (2010) 136805.

[13] S. Bertolazzi, J. Brivio, A. Kis, Stretching and breaking of ultrathin mos2, ACS Nano 5 (2011) 9703–9709.

[14] Z. Yin, H. Li, H. Li, L. Jiang, Y. Shi, Y. Sun, G. Lu, Q. Zhang, X. Chen, H. Zhang, Single-layer mos2 phototransistors, ACS Nano 6 (2012) 74–80.

[15] A. Splendiani, L. Sun, Y. Zhang, T. Li, J. Kim, C.-Y. Chim, G. Galli, F. Wang, Emerging photoluminescence in monolayer mos2, Nano Lett. 10 (2010) 1271–1275.

[16] R.J. Toh, Z. Sofer, M. Pumera, Catalytic properties of group 4 transition metal dichalcogenides (mx2; m = ti, zr, hf; x = s, se, te), J. Mater. Chem. A 4 (2016) 18322–18334.

[17] S. Kim, A. Konar, W.-S. Hwang, J.H. Lee, J. Lee, J. Yang, C. Jung, H. Kim, J.-B. Yoo, J.-Y. Choi, Y.W. Jin, S.Y. Lee, D. Jena, W. Choi, K. Kim, High-mobility and lowpower thin-film transistors based on multilayer mos2 crystals, Nat. Commun. 3 (2012) 1011.

[18] Q.H. Wang, K. Kalantar-Zadeh, A. Kis, J.N. Coleman, M.S. Strano, Electronics and optoelectronics of two-dimensional transition metal dichalcogenides, Nat. Nanotechnol. 7 (2012) 699–712.

[19] Yan, C.; Gan, L.; Zhou, X.; Guo, J.; Huang, W.; Huang, J.; Jin, B.; Xiong, J.; Zhai, T.; Li, Y. Space-Confined Chemical Vapor Deposition Synthesis of Ultrathin HfS2 Flakes for Optoelectronic Application. Adv. Funct. Mater. 2017, 27, 1702918.

[20] Zheng, B.; Chen, Y.; Wang, Z.; Qi, F.; Huang, Z.; Hao, X.; Li, P.; Zhang, W.; Li, Y. Vertically Oriented Few-Layered HfS2 Nanosheets: Growth Mechanism and Optical Properties. 2D Mater. 2016, 3, 035024.

[21] Wang, D.; Zhang, X.; Liu, H.; Meng, J.; Xia, J.; Yin, Z.; Wang, Y.; You, J.; Meng, X.-M. Epitaxial Growth of HfS2 on Sapphire by Chemical Vapor Deposition and Application for Photodetectors. 2D Mater 2017, 4, 031012.

[22] Wang, D.; Meng, J.; Zhang, X.; Guo, G.; Yin, Z.; Liu, H.; Cheng, L.; Gao, M.; You, J.; Wang, R. Selective Direct Growth of Atomic Layered HfS2 on Hexagonal Boron Nitride for High Performance Photodetectors. Chem. Mater. 2018, 30, 3819−3826.

[23] Zhu, Y.; Wang, X.; Zhang, M.; Cai, C.; Xie, L. Thickness and Temperature Dependent Electrical Properties of ZrS2 Thin Films Directly Grown on Hexagonal Boron Nitride. Nano Res. 2016, 9, 2931−2937.

[24] Ritala, M.; Niinistö, J. Atomic Layer Deposition. In Chemical Vapour Deposition: Precursors, Processes and Applications; Jones, A. C., Hitchman, M. L., Eds.; Royal Society of Chemistry: Cambridge, 2009; pp 158−206.

[25]Y. Guo, H. Wang, X. Feng, Y. Zhao, C. Liang, L. Yang, M. Li, Y. Zhang and W. Gao; 3D MXene microspheres with honeycomb architecture for tumor photothermal/photodynamic/ chemo combination therapy, Nanotechnology 32, 195701 (2021).

[26] J. D. Gouveia, G. Novell-Leruth, F. Vines, F. Illas, J R.B. Gomes, The Ti2CO2 MXene as a nucleobase 2D sensor: A first-principles study, Applied Surface Science 544 (2021) 148946.

[27] C. Wang H. Han, Y. Guo, Stabilities and electronic properties of vacancy-doped Ti2CO2,

Computational Materials Science 159 (2019) 127–135.

[28] L. Xiao-Hong, S. Xiang-Ying and Z. Rui-Zhou, Effect of vacancies on the structural and electronic properties of Ti2CO2, RSC Adv., 2019, 9, 27646.

[29] Y. Zhang, X-H. Zha, K. Luo, N. Qiu, Y. Zhou, J. He, Z. Chai, Z. Huang, Q. Huang, Y. Liang, and S. Du, Tuning the Electrical Conductivity of Ti2CO2 MXene by Varying the Layer Thickness and Applying Strains, J. Phys. Chem. C 2019, 123, 6802-6811.

[30] D. Sanchez-Portal, E. Artacho, J. M. Soler, Analysis of atomic orbital basis sets from the projection of plane-wave results, J. Phys.: Condens. Matter 8 (1996) 3859.

[31] J. P. Perdew, K. Burke, M. Ernzerhof, Generalized Gradient Approximation Made Simple, Phys. Rev. Lett. 77 (1996) 3865.

[32] A. D. Becke, Density-functional exchange-energy approximation with correct asymptotic behavior, Phys. Rev. A 38 (1988) 3098.

[33] O. A. Vydrov, T.V. Voorhis, Nonlocal van der Waals density functional: The simpler the better, J. Chem. Phys. 133 (2010) 244103.

[34] X. Gonze, C. Lee, Dynamical matrices, Born effective charges, dielectric permittivity tensors, and interatomic force constants from density-functional perturbation theory, Phys. Rev. B 55 (1997) 10355.

[35] X. Hu, L. Kou, and L. Sun, Stacking orders induced direct band gap in bilayer MoSe2-WSe2 lateral heterostructures, Sci. Rep. 6 (2016) 31122.

[36] K. Schwarz. K.; P. Blaha, Solid state calculations using WIEN2k. Comput. Mater. Sci. 2003, 28, 259.

[37] P. Giannozzi et. al. Advanced capabilities for materials modelling with Quantum Espresso. J. Phys.: Condens. Matter. 2017, 29, 465901.

[38] G.K.H. Madsen, D.J. Singh, Computer Physics Communications Volume 175, Issue 1, 2006, 67-71.

[39] J.P. Perdew, K. Burke, and M. Ernzerhof, Generalized gradient approximation made simple, Phys. Rev. Lett. 77, 3865 (1996).

[40] J.P. Perdew, Generalized gradient approximation for solids and their surfaces. Phys. Rev. Lett. 2008, 100, 136406.